Ultrastretchable Strain Sensors Using Carbon Black-Filled Elastomer Composites and Comparison of Capacitive Versus Resistive Sensors

Jun Shintake, Egor Piskarev, Seung Hee Jeong, and Dario Floreano*

The advent of soft robotics has led to the development of devices that harness the compliance and natural deformability of media with nonlinear elasticity. This has led to a need of batch-manufacturable soft sensors that can sustain large strains and maintain kinematic compatibility with the systems they track. In this article, an approach to address this challenge is presented with highly stretchable strain sensors that can operate at strains up to 500%. The sensors consist of a carbon black-filled elastomer composite that is batch manufactured using film-casting techniques and CO_2 laser ablation. This process facilitates the rapid multilayered fabrication of both capacitive and resistive sensing elements. When measuring capacitance, these sensors exhibit high linearity ($R^2 = 0.9995$), low hysteresis under cyclic loading with varying strain amplitude (50–500%), and high repeatability ($\geq 10^4$ cycles). The sensors possess gauge factors of 0.83–0.98 in capacitive mode and 1.62–3.37 in resistive mode.

1. Introduction

Systems that undergo large deformations, such as soft robots and wearable systems, are attracting increasing interest.[1,2] Soft and stretchable systems enable promising applications, such as robust and versatile robots,[3,4] devices for human robot interaction,[5,6] rehabilitation/ assistance,[7,8] and human monitoring.[9,10] In this context, strain sensing is important for detecting deformations and possibly controlling the system. Strain sensors that transduce large mechanical responses to electrical signals often require high stretchability (strain of more than 100%) for adequate estimation of the deforming

system.[11] Researchers have developed highly stretchable strain sensors made of compliant elastomers and various conductive materials, such as silver nanowire,[12] carbon nanotube (CNT),[13–18] carbon grease,[19] graphene,[20] graphite,[21] laser-carbonized polyimide,[22] conductive acrylic elastomer,[10] liquid metal,[23,24] ionic liquid,[25–27] and conductive fabric.[28] However, not all of these technologies can be manufactured in large scale at low cost.

Here, we propose the use of carbon black (CB)-filled elastomer composites for highly stretchable strain sensors (up to 500%) that can be batch manufactured at low cost. CBs are a type of low-cost conductive nanoparticle, which, when used as a filler in an elastomeric matrix, enhances the mechanical strength, abrasion resistance, UV resistance, and light absorbency of the composite.[29–31] The CB-filled elastomer can be printed in large areas by means of a layer-by-layer process,[32] with good wettability and high adhesion to silicone surfaces. Mixing various types of CBs and elastomers[33] gives material designers flexibility to achieve high compliance and stretchability.

Our layer-by-layer CB-filled elastomer fabrication process can be used to create resistive or capacitive sensors.[11] Resistive sensing relies on the piezoresistive effect and geometrical changes of electrodes, where mechanical strain causes a change in electrical resistivity. Capacitive sensing exploits changes of the capacitance between a pair of electrodes sandwiching a dielectric layer. Strain expands the area of the electrodes and reduces the thickness of the dielectric layer, leading to an increase of the capacitance. A recent review on strain sensors has pointed that resistive type strain sensors have high sensitivity but hysteresis and nonlinear response, while capacitive type strain sensors display excellent linearity and hysteresis performance but low sensitivity.[11] On the other hand, according to other literature, both resistive and capacitive type strain sensors show good linearity, low hysteresis, and repeatability.[10,13,15,28] Therefore, there is a lack of comprehensive knowledge of highly stretchable strain sensors that clarifies advantages and disadvantages of the two sensing methods. In addition, other characteristics, such as responses to different strain speed and temperature, have not yet been compared. This would result in difficulty when it is required to select an appropriate sensor

Dr. J. Shintake, Dr. S. H. Jeong, Prof. D. Floreano
Institute of Microengineering
School of Engineering
École Polytechnique Fédérale de Lausanne
Lausanne 1015, Switzerland
E-mail: dario.floreano@epfl.ch

E. Piskarev
Institute of Mechanical Engineering
School of Engineering
École Polytechnique Fédérale de Lausanne
Lausanne 1015, Switzerland

The ORCID identification number(s) for the author(s) of this article can be found under https://doi.org/10.1002/admt.201700284.

ADVANCED
SCIENCE NEWS
www.advancedsciencenews.com

ADVANCED
MATERIALS
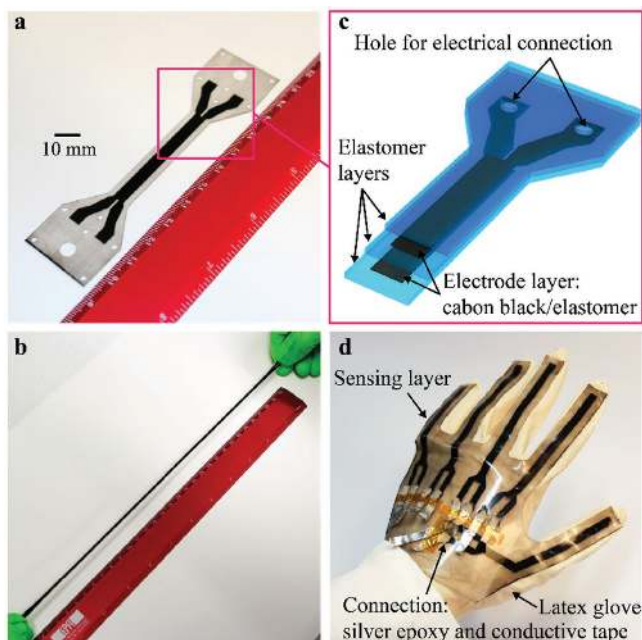**TECHNOLOGIES**
www.advmattechnol.de

Figure 1. Highly stretchable sensors with carbon black composite electrodes. a) A fabricated sensor for characterization. b) The sensor stretched up to 500% of strain. c) Structure of the sensor consists of electrode layers and dielectric layers. d) An intelligent glove integrating independently operated five sensors, which are fabricated in one single-layered structure.

type for a given target application. One approach to address this issue is to fabricate a sensor that measures strain through either capacitance or resistance and compare the performance of its sensing modes. However, to the best of the author's knowledge, there is no such study reported.

The strain sensor used in this study was made from CB-filled elastomer composite and silicone elastomer. The performance of its resistive and capacitive sensing modes was compared. We characterized the 1) sensor response for one cycle, 2) sensor response for multiple cycles, 3) sensor response for strain speed, and 4) sensor response for temperature. Thanks to the use of a highly compliant elastomer (Smooth-On, Ecoflex 00–30, modulus ≈125 kPa[34]), the sensor was able to measure strains up to 500% as shown in **Figure 1**a,b, which provided comparable or even larger strain measurement than other strain sensors.[11] The sensor was fabricated with a film-casting[35] process for laminating the electrode and elastomer layers, and laser ablation[32] for patterning the electrode design. These fabrication techniques provide a large area and are compatible with batch-type manufacturing (100 mm × 260 mm, see Figure S1, Supporting Information). The film-casting process provides control over both the elastomer and electrode thickness.

Though the sensor geometry used in this study was simple, the manufacturing process can be extended to arbitrary geometries. For example, the intelligent glove shown in Figure 1d has integrated sensors to detect the motion of every finger. The laser ablation process used in this study enables the rapid fabrication of multiple and complex sensor configurations.

2. Results and Discussion

The sensor consists of two overlapping electrode layers with a layer of dielectric between them (Figure 1c). It has in-plane geometric symmetry, facilitating the measurement of strain through either capacitance or resistance changes. Under uniaxial stress, the electrodes of the sensor are elongated and their surface area becomes larger, while the thickness of both the electrodes and the dielectric decreases, leading to changes in the capacitance and resistance. Assuming that both the dielectric and the electrode layers are incompressible, the deformation of the sensor under uniaxial stress can be expressed as[36]

$$l_e = l_{e0}(\varepsilon_1 + 1), \; w_e = \frac{w_{e0}}{\sqrt{\varepsilon_1 + 1}}, \; h_d = \frac{h_{d0}}{\sqrt{\varepsilon_1 + 1}} \tag{1}$$

where ε_1 is strain in the length (loading) direction (Figure S1h, Supporting Information), l_e the electrode length, w_e the electrode width, and h_d is the dielectric layer thickness. l_{e0}, w_{e0}, and h_{d0} are the equivalent quantities to l_e, w_e, and h_d in the reference configuration, respectively. Based on a simple parallel plate capacitor model, the capacitance of the sensor as a function of uniaxial strain is

$$C = \varepsilon_0\,\varepsilon_r\,\frac{l_e w_e}{h_d} = \varepsilon_0\,\varepsilon_r\,\frac{l_{e0} w_{e0}}{h_{d0}}(\varepsilon_1 + 1) = C_0(\varepsilon_1 + 1) \tag{2}$$

where ε_0 is the permittivity of free space, ε_r is the relative permittivity of the dielectric layer, and C_0 is the reference capacitance. Equation (2) suggests that the response of the sensor is linear with strain in the direction of loading. As also discussed in ref. [13], the gauge factor (GF), defined as $(\Delta C/C_0)/\varepsilon_1$, is predicted to be equal to 1.

As for the resistive response of the sensor, assuming that the cross sections of the electrode layers are uniform, the resistance can be expressed as

$$R = \rho\,\frac{l_{e0}}{w_{e0} h_{e0}}(\varepsilon_1 + 1)^2 = \frac{\rho}{\rho_0} R_0(\varepsilon_1 + 1)^2 \tag{3}$$

where ρ is the electrical resistivity of the conductive elastomer, ρ_0 the reference resistivity, h_{e0} the reference thickness of the electrode, and R_0 is the reference resistance. The resistivity of CB-filled elastomer composites changes under strain, due to breakdown and alignment of CB aggregates (i.e., conductive path).[37] Equation (3) predicts a nonlinear sensor response to uniaxial strain. The resistive sensing gauge factor GF_R is given as follows

$$GF_R = \frac{\Delta R}{R_0 \varepsilon_1} = \frac{1}{\varepsilon_1}\left\{\frac{\rho}{\rho_0}(\varepsilon_1 + 1)^2 - 1\right\} \tag{4}$$

Equation (4) suggests that the resistive sensing can have higher gauge factor than the capacitive sensing but its value changes as a function of the strain ε_1 (nonlinear sensor response).

The process used to fabricate sensor samples for characterization is detailed in the Experimental Section and Figure S1 (Supporting Information). This process is based on film casting

**ADVANCED
SCIENCE NEWS**
www.advancedsciencenews.com

**ADVANCED
MATERIALS
TECHNOLOGIES**
www.advmattechnol.de

the dielectric layers and the electrode layers one by one, using an applicator coater and a variable gap applicator. The electrode layer was ablated by a laser machine every time it was cast and cleaned with a solvent. The laser ablation removes mostly the electrode layer, while the dielectric layer on the bottom slightly loses its surface. The lost part of the dielectric layer was recovered by film casting of another dielectric layer in the subsequent steps. The sensor samples after all the film casting steps are shown in Figure S1g (Supporting Information). As we mentioned previously, they were batch manufactured with a large area (six samples per sheet). Subsequently, the samples were separated from the substrate, and each one was equipped with holding parts made of a rigid acrylic material, poly(methyl methacrylate) (PMMA). The holding parts are for the electrical connections and to ensure that only the active sensing part is stretched during characterization (see Figure S1f,h, Supporting Information). In the active part of the sensor, the overlapping electrodes are separated by a 125 mm thick dielectric and are 50 mm long and 5 mm wide. The unstrained values of capacitance and resistance for six fabricated samples were 45.3 ± 1.6 pF and 146.2 ± 18.6 kΩ, respectively.

We first assessed linearity and hysteresis of the fabricated sensor. One cycle of strain was applied to the sensor with strain amplitudes ranging from 50% to 500%. The result is plotted in **Figure 2**. As expected from Equation (2), for the capacitive sensor we observed linear response ($R^2 = 0.9995$) with the GF close to 1 at all the strain cycles: 0.98 (50%), 0.98 (100%), 0.96 (200%), 0.85 (300%), 0.83 (400%), and 0.86 (500%). The GF

reduction for larger strain may result from decrease of relative permittivity of the elastomer.[38] The reduction of relative permittivity decreases the capacitance, therefore the sensitivity. If that is the case, the GF defined as $(\Delta C/C_0)/\varepsilon_1$ is no more constant and will require the relative permittivity as a variable of strain. The capacitive response showed very little hysteresis. Drift error, the error of the sensor reading at 0% strain between before and after the stretch cycle, was 0.2% in 50% strain cycle and 4.2% in 500% strain cycle. On the other hand, the resistive sensor exhibited nonlinearity and variable GF over the different strain levels, as predicted by Equations (3) and 4: 1.62 (50%), 1.77 (100%), 1.74 (200%), 2.03 (300%), 2.51 (400%), and 3.37 (500%). The GF of the resistive sensing increased with the amplitude of the strain cycles. The higher resistive GF results from the change of both the resistivity and geometry of the CB electrodes. It should be noted that the gauge factor is determined by the type of materials and their concentration as has been suggested in highly sensitive strain gauges (e.g., refs. [39,40]). A lower concentration of the conductive particles in the composition should result in higher gauge factor. As for the hysteresis in the resistive sensing, we observed 24.1% drift error in 50% strain cycle and 35.9% drift error in 500% strain cycle. The large hysteresis of the resistive type sensor is most likely due to the viscoelasticity of CB-filled elastomer matrix, which can cause electromechanical delay in the sensor response.[41]

We then characterized the repeatability and durability of the sensor sample for 10 100 cycles with 200% strain. As shown
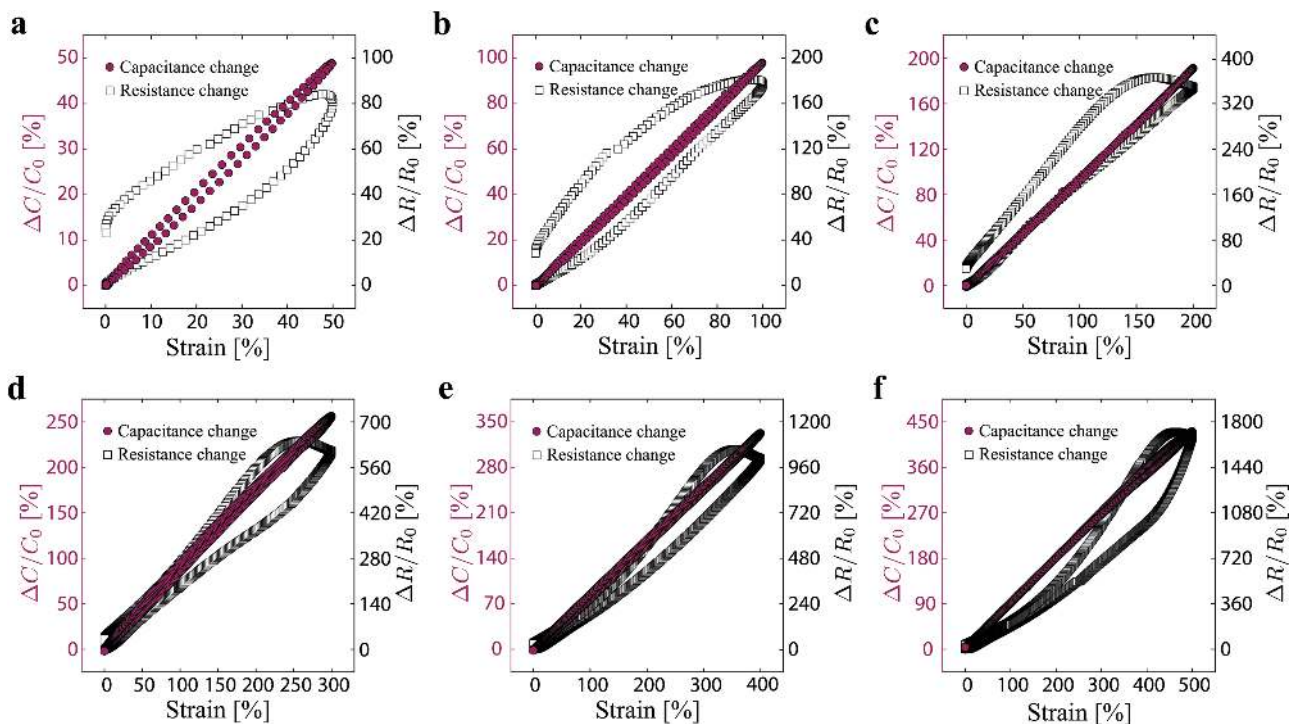

Figure 2. Measured sensor response of the fabricated sensor under one cycle strain for different strain amplitude: a) 50%, b) 100%, c) 200%, d) 300%, e) 400%, and f) 500%. The capacitive type exhibited linear sensor response ($R^2 = 0.9995$) and the gauge factor close to 1 for all the strain cycles, with very small hysteresis (0.2% drift error in 50% strain cycle and 4.2% drift error in 500% strain cycle). The resistive type showed nonlinearity and variable gauge factor over the strain cycles, with larger hysteresis compared to the capacitive one (24.1% drift error in 50% strain cycle and 35.9% drift error in 500%).
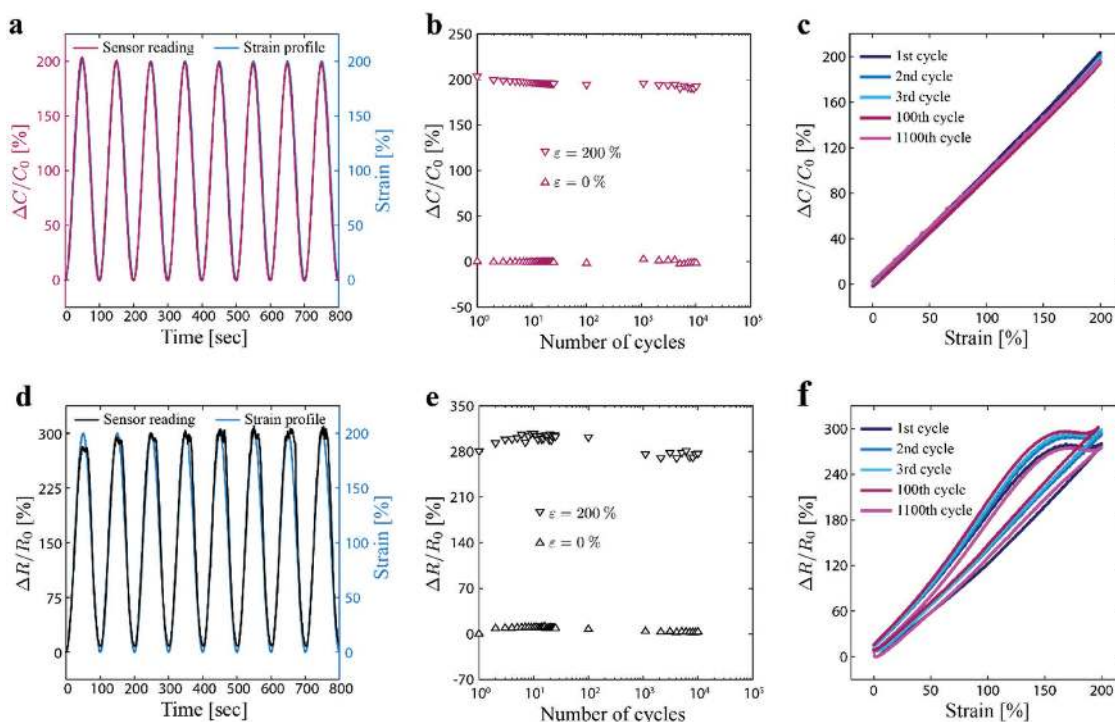
ADVANCED
SCIENCE NEWS
www.advancedsciencenews.com

ADVANCED
MATERIALS
TECHNOLOGIES
www.advmattechnol.de

Figure 3. Measured sensor response during 10 100 strain cycles with 200% strain. a) Capacitance change and strain profile as functions of time at the first eight cycles. b) Capacitance change at 200% and 0% strain as a function of number of cycles. The drift error at the last cycle was −1.7% at 0% strain and −10.8% at 200% strain. c) Capacitance change at multiple cycles. d) Resistance change and strain profile as functions of time at the first eight cycles. e) Resistance change at 200% and 0% strain as a function of number of cycles. The drift error at the last cycle was 2.9% at 0% strain and −3.8% at 200% strain. f) Resistive change at multiple cycles.

in **Figure 3**a–c, the capacitive type sensor displayed high repeatability and durability over the cyclic tests. The drift error at the last cycle was −1.7% at 0% strain and −10.8% at 200% strain. On the other hand, the resistive type sensor (Figure 3d–f) displayed lower repeatability and the response was more varied over the entire set of cycles. The variation of the resistance change (Figure 3d–f) indicates an increase at the early part of the strain cycles and subsequent stabilization at the latter part. This behavior is observed in other resistive strain sensors.[15] This may result from dynamic orientation change

of CB aggregates (i.e., conductive path) suspended in the polymer network.[37] The drift error at the last cycle was 2.9% at 0% strain and −3.8% at 200% strain. In addition, throughout the test we did not observe any noticeable buckling of the electrode layer that appears in other types of conductive polymer composites.[42,43]

Since soft and stretchable systems often undergo deformations at different rates, sensor response under different strain speed is an important aspect that gives us the insight to determine the nature of potential applications. **Figure 4**a,b plots the
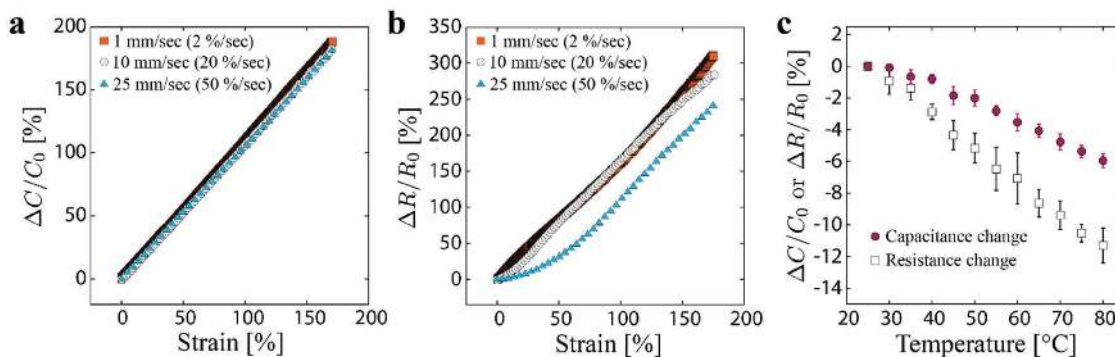

Figure 4. a) Measured capacitance change under different strain speed. The sensor response is stable for all the speeds. b) Measured resistance change under different strain speed. The sensor response showed delay at higher speeds. c) Measured sensor response as a function of temperature. Values are the average of three measurements. The capacitive sensor showed roughly two times smaller change than the resistive sensor; at 80 °C, −6.0% for the capacitance change and −11.3% for the resistance change.

**ADVANCED
SCIENCE NEWS**
www.advancedsciencenews.com

**ADVANCED
MATERIALS
TECHNOLOGIES**
www.advmattechnol.de

Table 1. Performance comparison of highly stretchable strain sensors developed in this study and results in literature.

Sensor type	Reference	Materials	Stretchability (%)	Gauge factor	Strain rate (%/s)	Number of cycles	Hysteresis	Linearity
Capacitive	This study	Ecoflex-CB	500	0.83–0.98	50	10 100	Low	Linear
	[10]	PDMS-conductive acrylic	150	0.9	4.6	1000	Low	Linear
	[13]	PDMS-CNT	300	≈1	10	10 000	Low	Linear
	[28]	Ecoflex-conductive fabric	150	1.23	37	1000	Low	Linear
	[21]	Dragonskin-graphite	250	0.54–1.13	1.7	1000	Low	Linear
	[26]	Dragonskin-ionic liquid	250	0.35	25	20	Low	Nonlinear
Resistive	This study	Ecoflex-CB	500	1.62–3.37	50	10 100	High	Nonlinear
	[19]	Ecoflex-carbon grease	450	3.8	16.7	N/A	High	Nonlinear
	[15]	Ecoflex-CNT	500	1.75	40	2000	Low	Linear
	[27]	Ecoflex-ionic liquid	300	1.75–3.75	10	3000	Low	Nonlinear
	[22]	PDMS-carbonized polyimide	100	50–20 000	N/A	1000	N/A	Nonlinear

capacitive sensor response and the resistive sensor response at different strain speeds, respectively. The strain speeds were 1 mm s^{-1} (2% s^{-1}), 10 mm s^{-1} (20% s^{-1}), and 25 mm s^{-1} (50% s^{-1}). We observed stable sensor response for the capacitance change at all the speeds we tested. The strain speed 50% s^{-1} corresponds to 0.14 Hz of cycle frequency in this experiment. Given a highly stretchable capacitive strain sensor that has similar performance (**Table 1**, ref. [28]) exhibits stable response up to 27 Hz with 10% strain amplitude, our sensor in capacitive mode is expected to function at comparable frequencies higher than the current result. As for the resistive sensor response, its response was relatively stable at moderate speeds (up to 10 mm s^{-1}) but it showed significant delay at 25 mm s^{-1}. This suggests that the frequency response of the sensor in resistive mode will be lower than the capacitive one. The reason for the delay may be due to the viscoelastic nature of the electrode (which is also likely responsible for the hysterics shown in Figure 2). The capacitive sensor works better than the resistive sensor at higher strain rates because the dielectric layer has lower hysteresis than the CB electrodes.

We also investigated the influence of temperature on the unstrained capacitance and resistance of the sensors. The sensor was placed on a hot plate under zero strain, and the temperature was increased from 25 °C (room temperature) to 80 °C. Both the capacitive and resistive type sensors showed reduction in their respective electrical properties with the temperature increase (Figure 4c). However, the amount of change was different for the two sensors. The capacitive sensor displayed half the percentage change of the resistive sensor (at 80 °C, −6.0% for the capacitive type and −11.3% for the resistive type). The observed change in sensor measurements with temperature may be attributed to the coupling between their thermal, electrical, and mechanical properties. The reduction of capacitance was likely driven by the decreasing polymer network density with increasing temperature.[44] The reduction in polymer network density decreases the relative permittivity. On the other hand, uniform thermal strains in the principal directions should cause an increase in relative capacitance, assuming that thermal expansion is isotropic. However, the observed decrease in relative capacitance with increased temperature would suggest that the thermoelectric response of the sensors dominate

their thermomechanical response. The reduction of resistance has been characterized as a negative temperature coefficient (NTC) effect observed in certain types of conductive polymers that lowers their resistivity.[45–47] In CB-filled elastomer composites, NTC is exhibited when the size of the particles is small and their concentration is near the percolation threshold.[48] There are mainly three reasons associated with the decrease in resistivity: the thermal emission of electrons between neighboring CB particles, the particle realignment, and the oxidative crosslinking at the surface.[47,49] Thermal expansion of elastomer tends to destroy conductive pathways of CBs, leading to an increase in the resistivity. However, this effect is marginal and cannot overcome the three effects mentioned above, resulting in an NTC effect.[47]

These experiments assess, for the first time, the advantages and disadvantages of resistive and capacitive highly stretchable strain sensors using the same geometry, materials, and processing methods. The resistive type sensor has higher gauge factors and thus is better suited for highly sensitive strain detection. Also, it has lower cost and fabrication time because it requires only one electrode layer. Implementing resistance measurement is also typically easier than capacitance measurement in a mechatronic system. Once implemented, however, the capacitive sensor had comparable or better performance than the resistive sensor in nearly every metric we tested. Compared to the resistive sensor, the capacitive sensor displayed better linearity, less hysteresis, and more repeatability. It was also more consistent over changes in strain speed. It was only exceeded by the resistive sensor in its gauge factor.

These results provide evidence for a quantitative comparison between highly stretchable resistive and capacitive sensing, and provide new insight on strain speed characteristics and thermal dependences. The performance of our sensors is summarized in Table 1 and compared to other highly stretchable strain sensors found in the literature. From this table, it is readily seen that the performance of our sensors is comparable to other sensors of the same type in both capacitive and resistive sensing methods.

To validate the potential applications of our highly stretchable strain sensors for soft and deformable systems, we prototyped an intelligent latex glove with a sensing layer that measures
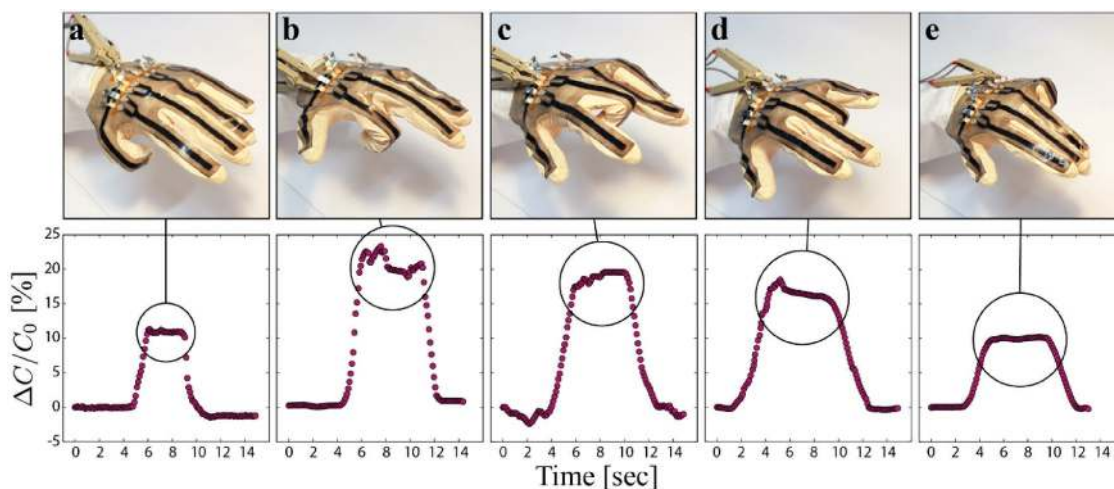
1700284 (5 of 8)

**ADVANCED
SCIENCE NEWS**
www.advancedsciencenews.com

**ADVANCED
MATERIALS
TECHNOLOGIES**
www.advmattechnol.de

Figure 5. Demonstration of capacitive type sensors in an intelligent glove fabricated with capacitance strain sensors over the a) thumb, b) index, c) middle, d) third, and e) fourth fingers.

the bending of each digit (Figure 1d). The glove includes an independent sensor covering each finger. These sensors were fabricated in a single layer using the same process used for the sensors characterized in this work (see Experimental Section). This hand-shaped sensing layer was bonded to the glove with silicone glue (Dow Corning, 734 RTV). The sensors were employed in the capacitive mode due to its superior performance revealed by the experimental characterization described above. The sensors were able to detect the motion of the fingers (**Figure 5**) through changes in capacitance. As expected, increasing the flexion angle of the finger joints increased the capacitance. This result also showed that the sensors are stable for a static load which is visible especially in Figure 5e.

3. Conclusion

We have developed highly stretchable strain sensors using a CB-filled elastomer composite and silicone elastomer. The use of this composite enabled the sensors to function at strains as high as 500%. Owing to the layered, film-casting fabrication approach, multilayered sensors were produced in a large area, low-cost batch manufacturing process. The resulting sensors can measure strain through either capacitance or resistance. These sensors were tested to over 10 000 cycles without failure. With the aid of laser ablation, the fabrication process we used is adaptable to design planar sensor geometries for diverse applications. We demonstrated this in the intelligent glove.

The capacitive type sensor displayed superior or equal performance compared to the resistive sensor in all metrics except the gauge factor. The capacitive sensor had high linearity ($R^2 = 0.9995$), low hysteresis, and high repeatability. Its performance was consistent across strain rates as high as 50% s^{-1}. These results are comparable to other highly stretchable sensors in the literature. They also illustrate the high performance of highly stretchable strain sensors made of CB-filled elastomer and provide insights for choosing the most appropriate sensor type for the desired application. In particular, the sensors made

with CB-filled elastomer composite presented here may be used in a wide range of sensorized soft robots and wearable systems.

4. Experimental Section

CB-Filled Elastomer Composite for Electrodes: The CB composite was prepared by mixing conductive nanoparticles (AkzoNobel, Ketjenblack EC-300J) and a liquid silicone elastomer (Smooth-On, Ecoflex 00–30) by weight ratio of 1:10 (CB:Ecoflex), in a planetary centrifugal mixer (Thinky, ARE-250) for 10 min at 2000 rpm.

CB-Filled Elastomer Composite for Interconnection with Wires: The conductive mixture was prepared by adapting the recipe presented in ref. [50]. The preparation was done by mixing a CB (Cabot, XC-72) and a liquid silicone elastomer (Dow Corning, Sylgard 184). They were mixed with mass ratio of CB: Base oligomer: Curing agent = 1:6:0.6 in the planetary centrifugal mixer for 5 min at 2000 rpm.

Sensor Sample and Intelligent Glove Fabrication: The fabrication process of the sensors used in this study is shown in Figure S1 (Supporting Information). This process features a large working area (100 mm × 260 mm) and batch fabrication (six samples in our study, Figure S1g, Supporting Information). First, a thin-film elastomer of 200 µm thickness was cast on a polyethylene terephthalate film using an applicator coater (Zehntner, ZUA2000) and a variable gap applicator (Zehntner, ZAA2300) (Figure S1a,Supporting Information). The elastomer layer was then cured in an oven for 30 min at 80 °C. Subsequently, the electrode composite layer was cast and cured in the same manner as the elastomer layer (Figure S1b, Supporting Information). The thickness of the electrode layer was ≈20 µm after curing. The electrode layer was then ablated using a laser engraver (Trotec, Speedy 300) to obtain the sensor electrode geometry (Figure S1c, Supporting Information), and then the sample surface was cleaned with a solvent (isopropyl alcohol). The laser ablation also slightly removes the surface part of the elastomer layer during the ablation, but it will be recovered by the next step casting another elastomer layer on top. After that, the aforementioned steps (Figure S1a–c, Supporting Information) were repeated, and the top elastomer layer thickness of 500 µm was cast (Figure S1d, Supporting Information). The entire sheet was then cut by the laser engraver to separate each sensor and make holes for electrical interfacing and holding parts. (Figure S1e, Supporting Information). Finally, holding parts made of acrylic plates (PMMA) were assembled, and the CB-filled elastomer composite (XC-72) was filled into the holes for wiring to establish the electrical connections using a conductive tape (Figure S1f,

**ADVANCED
SCIENCE NEWS**

www.advancedsciencenews.com

**ADVANCED
MATERIALS
TECHNOLOGIES**

www.advmattechnol.de

Supporting Information). For sample characterization, the holding parts were made with screw holes to anchor the sensor terminals (Figure S1h, Supporting Information). The fabrication of the intelligent glove (Figure 1d) followed the same process described above, except for the use of a conductive silver epoxy (Amepox, ELECTON 40AC) instead of the XC-72 composite.

Experimental Setup for Sensor Characterization: The sensor was attached to a linear motorized stage (Zaber, A-LST-1500D) that uniaxially loaded the sample. An LCR meter (Hioki, IM3523) was used to measure both capacitance and resistance values of the sensor. Both the stage and the LCR meter were controlled through a LabVIEW interface which stored the data of strain, capacitance, and resistance at the sampling rate of 10 Hz. In the LCR meter, the test frequency was set to 1 kHz. The sensor sample had four electrical terminals (Figure S1h, Supporting Information) to measure the capacitance (use connections 1–2 or 3–4) and the resistance (use connections 1–3 or 2–4). In this study, connections 3–4 were used for the capacitive sensing and connections 1–3 for the resistive sensing.

In one cycle strain measurement (Figure 2), the cycle frequencies were 0.125, 0.0625, 0.03125, 0.020833, 0.015625, and 0.0125 Hz for 50%, 100%, 200%, 300%, 400%, and 500% strain amplitude, respectively. A time interval of 30 min was provided between each cycle to eliminate drift in the sensor response, particularly for resistive sensing. Linearity of the sensor response (coefficient of determination R^2) was calculated by fitting the data using MATLAB 2015b. The cycle frequency of 0.1 Hz was used for measurements taken in the case of cyclic loading (Figure 3). When studying the thermal effects (Figure 4c), the sensor was placed on a hot plate (Torrey Pines Scientific, HS65-2) where the associated thermocouple was attached to the sensor so that it was heated to the target temperature. In the demonstration of the intelligent glove (Figure 5), sensor response of every finger was measured individually.

Supporting Information

Supporting Information is available from the Wiley Online Library or from the author.

Conflict of Interest

The authors declare no conflict of interest.

[1] D. Rus, M. T. Tolley, *Nature* **2015**, *521*, 467.
[2] W. Zeng, L. Shu, Q. Li, S. Chen, F. Wang, X.-M. Tao, *Adv. Mater.* **2014**, *25*, 5310.
[3] M. T. Tolley, R. F. Shepherd, B. Mosadegh, K. C. Galloway, M. Wehner, M. Karpelson, R. J. Wood, G. M. Whitesides, *Soft Rob.* **2014**, *1*, 213.

[4] J. Shintake, S. Rosset, B. Schubert, D. Floreano, H. Shea, *Adv. Mater.* **2016**, *28*, 231.
[5] S. Sanan, M. H. Ornstein, C. G. Atkeson, in *Annual Int. Conf. of the IEEE Engineering in Medicine and Biology Society*, Boston, MA, USA **2011**.
[6] A. Alspach, J. Kim, K. Yamane, in *IEEE-RAS 15th Int.Conf. on Humanoid Robots*, Seoul, South Korea **2015**.
[7] P. Polygerinos, Z. Wang, K. C. Galloway, R. J. Wood, C. J. Walsh, *Rob. Auton. Syst.* **2015**, *73*, 135.
[8] M. Wehner, B. Quinlivan, P. M. Aubin, E. Martinez-Villalpando, M. Baumann, L. Stirling, K. Holt, R. J. Wood, C. Walsh, in *IEEE Int. Conf. on Robotics and Automation*, Karlsruhe, Germany **2013**.
[9] F. Lorussi, E. P. Scilingo, M. Tesconi, A. Tognetti, D. D. Rossi, *IEEE Trans. Inf. Technol. Biomed.* **2005**, *9*, 372.
[10] M. D. Bartlett, E. J. Markvicka, C. Majidi, *Adv. Funct. Mater.* **2016**, *26*, 8496.
[11] M. Amjadi, K.-U. Kyung, I. Park, M. Sitti, *Adv. Funct. Mater.* **2016**, *26*, 1678.
[12] B.-U. Hwang, J.-H. Lee, T. Q. Trung, E. Roh, D.-I. Kim, S.-W. Kim, N.-E. Lee, *ACS Nano* **2015**, *9*, 8801.
[13] L. Cai, L. Song, P. Luan, Q. Zhang, N. Zhang, Q. Gao, D. Zhao, X. Zhang, M. Tu, F. Yang, W. Zhou, Q. Fan, J. Luo, W. Zhou, P. M. Ajayan, S. Xie, *Sci. Rep.* **2013**, *3*, 3048.
[14] Y. Li, Y. Shang, X. He, Q. Peng, S. Du, E. Shi, S. Wu, Z. Li, P. Li, A. Cao, *ACS Nano* **2013**, *7*, 8128.
[15] M. Amjadi, Y. J. Yoon, I. Park, *Nanotechnology* **2015**, *26*, 375501.
[16] Z. F. Liu, S. Fang, F. A. Moura, J. N. Ding, N. Jiang, J. Di, M. Zhang, X. Lepró, D. S. Galvão, C. S. Haines, N. Y. Yuan, S. G. Yin, D. W. Lee, R. Wang, H. Y. Wang, W. Lv, C. Dong, R. C. Zhang, M. J. Chen, Q. Yin, Y. T. Chong, R. Zhang, X. Wang, M. D. Lima, R. Ovalle-Robles, D. Qian, H. Lu, R. H. Baughman, *Science* **2015**, *349*, 400.
[17] E. Roh, B.-U. Hwang, D. Kim, B.-Y. Kim, N.-E. Lee, *ACS Nano* **2015**, *9*, 6252.
[18] K. Suzuki, K. Yataka, Y. Okumiya, S. Sakakibara, K. Sako, H. Mimura, Y. Inoue, *ACS Sens.* **2016**, *1*, 817.
[19] J. T. Muth, D. M. Vogt, R. L. Truby, Y. Mengüç, D. B. Kolesky, R. J. Wood, J. A. Lewis, *Adv. Mater.* **2014**. *26*, 6307.
[20] J. Jin Park, W. J. Hyun, S. C. Mun, Y. T. Park, O. O. Park, *ACS Appl. Mater. Interfaces* **2015**, *7*, 6317.
[21] E. L. White, M. C. Yuen, J. C. Case, R. K. Kramer, *Adv. Mater. Technol.* **2017**, *2*, 1700072.
[22] R. Rahimi, M. Ochoa, W. Yu, B. Ziaie, *ACS Appl. Mater. Interfaces* **2015**, *7*, 4463.
[23] Y. Mengüç, Y.-L. Park, E. Martinez-Villalpando, P. Aubin, M. Zisook, L. Stirling, R. J. Wood, C. J. Walsh, in *IEEE Int. Conf. on Robotics and Automation*, Karlsruhe, Germany **2013**.
[24] S. Zhu, J.-H. So, R. Mays, S. Desai, W. R. Barnes, B. Pourdeyhimi, M. D. Dickey, *Adv. Funct. Mater.* **2013**, *23*, 2308.
[25] J.-B. Chossat, Y.-L. Park, R. J. Wood, V. Duchaine, *IEEE Sens. J.* **2013**, *13*, 3405.
[26] A. Frutiger, J. T. Muth, D. M. Vogt, Y. Mengüç, A. Campo, A. D. Valentine, C. J. Walsh, J. A. Lewis, *Adv. Mater.* **2015**, *27*, 2440.
[27] D. Y. Choi, M. H. Kim, Y. S. Oh, S.-H. Jung, J. H. Jung, H. J. Sung, H. W. Lee, H. M. Lee, *ACS Appl. Mater. Interfaces* **2017**, *9*, 1770.
[28] A. Atalay, V. Sanchez, O. Atalay, D. M. Vogt, F. Haufe, R. J. Wood, C. J. Walsh, *Adv. Mater. Technol.* **2017**, *2*, 1700136.
[29] K. Tsunoda, J. J. C. Busfield, C. K. L. Davies, A. G. Thomas, *J. Mater. Sci.* **2000**, *35*, 5187.
[30] H. Liang, Y. Fukahori, A. G. Thomas, J. J. C. Busfield, *Wear* **2009**, *266*, 288.
[31] J. Accorsi, E. Romero, *Plast. Eng.* **1995**, *51*, 29.
[32] O. A. Araromi, S. Rosset, H. Shea, *ACS Appl. Mater. Interfaces* **2015**, *7*, 18046.

[33] J. C. Huang, *Adv. Polym. Technol.* **2002**, *21*, 299.

[34] Y.-L. Park, C. Majidi, R. Kramer, P. Bérard, R. J. Wood, *J. Micromech. Microeng.* **2010**, *20*, 125029.

[35] S. Rosset, O. A. Araromi, S. Schlatter, H. Shea, *J. Vis. Exp.* **2016**, 53423.

[36] M. H. Sadd, *Elasticity: Theory, Applications, and Numerics*, Academic Press, Cambridge, MA, USA **2009**.

[37] K. Yamaguchi, J. J. C. Busfield, A. G. Thomas, *J. Polym. Sci., Part B: Polym. Phys.* **2003**, *41*, 2079.

[38] V. L. Tagarielli, R. Hildick-Smith, J. E. Huber, *Int. J. Solids Struct.* **2012**, *49*, 3409.

[39] M. Hempel, D. Nezich, J. Kong, M. Hofmann, *Nano Lett.* **2012**, *12*, 5714.

[40] X. Li, T. Yang, Y. Yang, J. Zhu, L. Li, F. E. Alam, X. Li, K. Wang, H. Cheng, C. T. Lin, Y. Fang, H. Zhu, *Adv. Funct. Mater.* **2016**, *26*, 1322.

[41] A. Lion, *Continuum Mech. Thermodyn.* **1996**, *8*, 153.

[42] D. J. Lipomi, M. Vosgueritchian, B. C.-K. Tee, S. L. Hellstrom, J. A. Lee, C. H. Fox, Z. Bao, *Nat. Nanotechnol.* **2011**, *6*, 788.

[43] J. Shi, X. Li, H. Cheng, Z. Liu, L. Zhao, T. Yang, Z. Dai, Z. Cheng, E. Shi, L. Yang, Z. Zhang, A. Cao, H. Zhu, Y. Fang, *Adv. Funct. Mater.* **2016**, *26*, 2078.

[44] G. Williams, *Dielectric Properties of Polymers. Materials Science and Technology*, Wiley-VCH, Weinheim, Germany **2006**.

[45] Z.-D. Xiang, T. Chen, Z.-M. Li, X.-C. Bian, *Macromol. Mater. Eng.* **2009**, *294*, 91.

[46] N. C. Das, T. K. Chaki, D. Khastgir, *Carbon* **2002**, *40*, 807.

[47] K. P. Sau, T. K. Chaki, D. Khastgir, *J. Appl. Polym. Sci.* **1999**, *71*, 887.

[48] J. Zhang, S. Feng, *J. Appl. Polym. Sci.* **2003**, *90*, 3889.

[49] B. Mettson, B. Stenberg, *Rubber Chem. Technol.* **1992**, *65*, 315.

[50] F. M. Yaul, V. Bulovic, J. H. Lang, *IEEE J. Microelectromech. Syst.* **2012**, *21*, 897.